NANO LETTERS

pubs.acs.org/NanoLett Letter

Raman Spectroscopic Probe for Nonlinear MoS_2 Nanoelectromechanical Resonators

Rui Yang,* S M Enamul Hoque Yousuf, Jaesung Lee, Pengcheng Zhang, Zuheng Liu, and Philip X.-L. Feng*

Cite This: *Nano Lett.* 2022, 22, 5780−5787 Read Online

ACCESS | Metrics & More | Article Recommendations | Supporting Information

ABSTRACT: Resonant nanoelectromechanical systems (NEMS) enabled by two-dimensional (2D) semiconductors have been actively explored and engineered for making ultrascaled transducers toward applications in ultralow-power signal processing, communication, and sensing. Although the transduction of miniscule resonant motions has been achieved by low-noise optical or electronic techniques, direct probing of strain in vibrating 2D semiconductor membranes and the interplay between the spectroscopic and mechanical properties are still largely unexplored. Here, we experimentally demonstrate dynamical phonon softening in atomically thin molybdenum disulfide (MoS_2) NEMS resonators by directly coupling Raman spectroscopy with optical interferometry resonance motion detection. In single-layer, bilayer, and trilayer (1L to 3L) MoS_2 circular membrane NEMS resonators, we show that high-amplitude nonlinear resonances can enhance the Raman signal amplitude, as well as introduce Raman modes softening up to 0.8 cm^{-1}. These results shall pave the way for engineering the coupling and control between collective mechanical vibrations and Raman modes of the constituent crystals in 2D transducers.

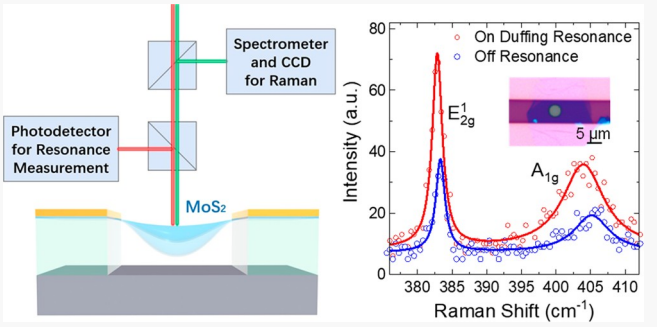

KEYWORDS: *2D materials, nanoelectromechanical systems (NEMS), Raman, nonlinear, resonator*

Resonant nanoelectromechanical systems (NEMS) based on two-dimensional (2D) materials have attracted tremendous interest due to their atomic-scale thicknesses, high Young's moduli, and ultrahigh strain limits.[1,2] Graphene NEMS resonators have been explored using detection techniques such as optical interferometry,[3,4] frequency mixing detection,[5,6] and direct radio frequency (RF) electrical readout.[7,8] Beyond graphene, semiconductor NEMS resonators in transition metal dichalcogenides (TMDCs) such as molybdenum disulfide (MoS_2) have also been extensively studied with optical interferometry measurements showing thermomechanical resonance frequencies up to 60 MHz in the very high frequency (VHF) band, quality (Q) factor up to 1050 at room temperature and 47 000 at cryogenic temperature, a frequency tuning range of 150% using strain, and a broad linear dynamic range up to 110 dB.[9−13] As a 2D semiconductor, MoS_2 also has a higher piezoresistive gauge factor than graphene,[14] thus 2D MoS_2 NEMS resonators can exhibit strong electromechanical coupling with the channel conductance not only modulated by the displacement but also by the dynamic strain.[15] Using such electromechanical coupling effects, all-electrical signal transduction of 2D MoS_2 NEMS resonators has been achieved.[16−18]

While these demonstrations of resonance detection show the device vibration amplitude, frequency, Q factor, and so forth, they do not provide direct information on the vibration-induced dynamic strain and other important intrinsic physical effects, which are also essential for understanding the dynamics of the crystal lattices in these resonators. Directly probing the dynamic strain in 2D NEMS resonators could be especially useful when the motion detection responsivity in optical interferometry is low under certain conditions of parameters including the vacuum gap and resonator thickness,[19] when the dynamic strain is coupled to the conductance change in 2D semiconductors or for studying the strain-mediated coupling between the collective mechanical vibrations and spins or quantum dots.[20,21] Dynamic strain has also been used to control quantum systems such as negatively charged silicon vacancy centers, as shown by the optically detected acoustic resonance (ODAR) measurements.[22] Static tensile strain in 2D MoS_2 can be probed by photoluminescence or Raman spectroscopy due to the bandgap narrowing and phonon softening effects, respectively.[23−27] The strain-sensitive E_{2g}^1

Received: March 28, 2022
Revised: June 28, 2022
Published: July 6, 2022

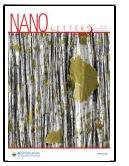

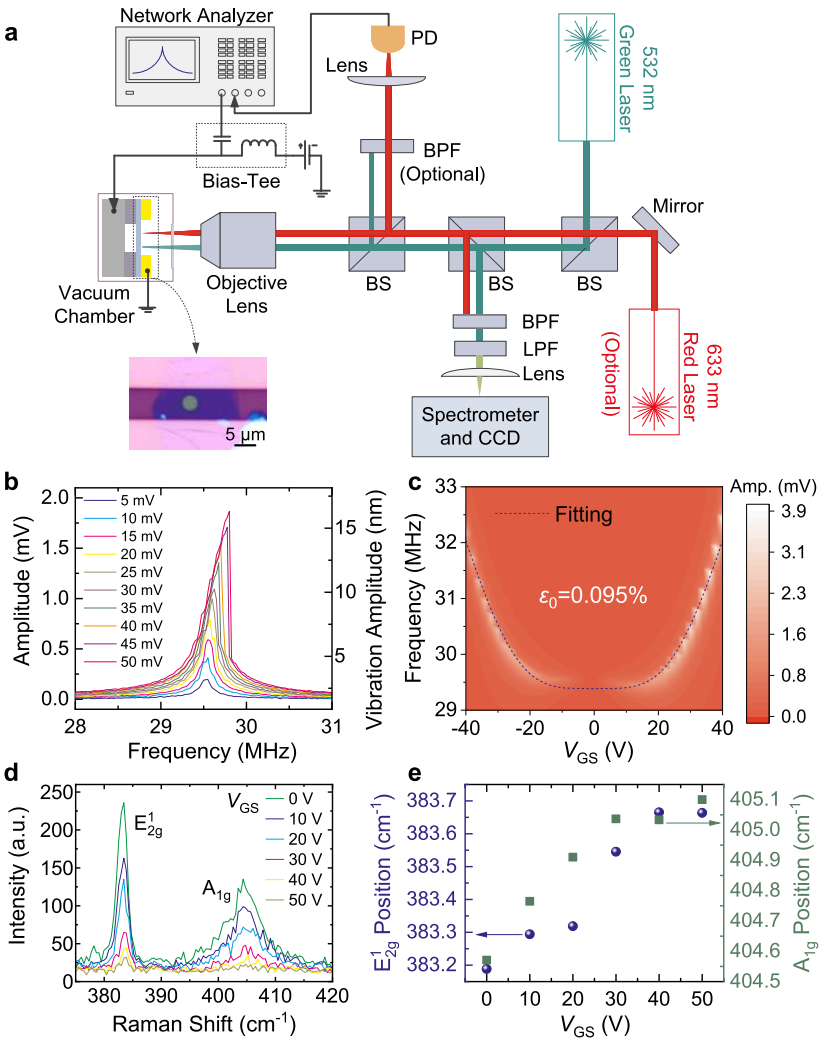

Figure 1. Measurement system with resonance and Raman signals measured from MoS_2 NEMS resonators. (a) Schematic illustration showing the experimental system for simultaneous interferometric resonance measurement (using the 633 nm laser) and Raman spectroscopy measurement (using the 532 nm laser). The optical image of a 2L circular drumhead MoS_2 NEMS resonator with diameter d = 4 μm is shown on the lower left corner. (b) Measured resonances at V_{GS} = 10 V with different RF driving voltages, showing the transition from linear to nonlinear resonances, for the 2L MoS_2 NEMS resonator shown in (a). (c) Resonance signal amplitude shown in color scale, at different V_{GS} and with ν_{RF} fixed at 20 mV. The fitting of the resonance frequency tuning is shown by the blue dashed line from which the initial strain of ε_0 = 0.095% is extracted. (d) Raman spectra of the suspended 2L MoS_2 measured at varying V_{GS}. (e) Summarized $E_{2g}{}^1$ (left axis) and A_{1g} (right axis) peak positions at different V_{GS}.

Raman mode is insensitive to gate-voltage-induced changes in electron concentration, while the strain-insensitive A_{1g} mode is more sensitive to electron concentration change.[28,29] Raman spectroscopy has been used to measure the dynamic strain in graphene resonators.[30,31] The exciton-optomechanical coupling has also been observed in suspended 1L $MoSe_2$.[32] However, crystal lattice phonon signatures in vibrating 2D semiconductor NEMS resonators have not been directly measured.

In this work, we experimentally probe the coupling between the collective nanomechanical vibrations at the device level and the phonon modes at the crystal lattice level by performing simultaneous optical interferometry resonance detection and Raman spectroscopy measurements in single-layer (1L), bilayer (2L), and trilayer (3L) MoS_2 circular membrane NEMS resonators. These 2D MoS_2 NEMS resonators exhibit Duffing nonlinear resonances with high vibration amplitude, and their Raman modes shift toward smaller wavenumbers when driven on resonances, showing a phonon softening effect. We demonstrate a Raman peak shift up to 0.8 cm^{-1}, and a dynamic strain up to 0.51% in these 2D MoS_2 resonators. The devices also show an increase of the Raman peak amplitude when driven at a large vibration amplitude, which is attributed to changes in the membrane equilibrium position. These results open new possibilities for engineering the mesoscopic dynamics of 2D semiconductor NEMS.

We develop a custom-built measurement system with coupled optical interferometry and Raman spectroscopy, by using a 633 nm He−Ne laser with a spot size of about 1 μm for resonance measurements,[10] and a 532 nm semiconductor laser with a spot size of about 680 nm for Raman scattering and phonon mode measurements (Figure 1a). The lasers are focused close to the middle of the suspended membranes during the measurements. Note that the resonance measurement can also be performed using the 532 nm laser, albeit with a more noticeable parasitic heating effect. The 2D MoS_2 resonators are circular membranes fully covering microtrenches on the 290 nm SiO_2-on-Si substrate. Fabrication of

https://doi.org/10.1021/acs.nanolett.2c01250
Nano Lett. 2022, 22, 5780−5787

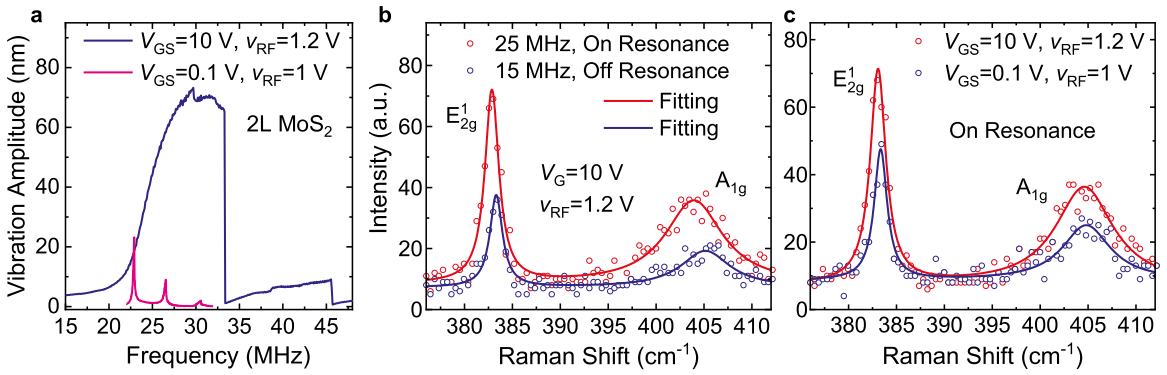

Figure 2. Resonances and Raman spectra measured from the same 2L circular drumhead MoS_2 NEMS resonator as shown in Figure 1. (a) Resonance spectra measured with DC gate voltage V_{GS} = 10 V, RF voltage v_{RF} = 1.2 V (blue curve), showing strongly nonlinear resonances, and with V_{GS} = 0.1 V, v_{RF} = 1 V (magenta curve), showing linear resonances. (b) Raman spectra with the device driven at V_{GS} = 10 V, v_{RF} = 1.2 V, showing $E_{2g}{}^1$ and A_{1g} modes, when the driving frequencies are off resonance (blue symbols) and on resonance (red symbols). (c) Raman spectra with the device driven at the resonance frequency, when the driving amplitudes are V_{GS} = 0.1 V, v_{RF} = 1 V (blue symbols), and V_{GS} = 10 V, v_{RF} = 1.2 V (red symbols). The red and blue lines in (b,c) show the fitting curves for the red and blue data points, respectively.

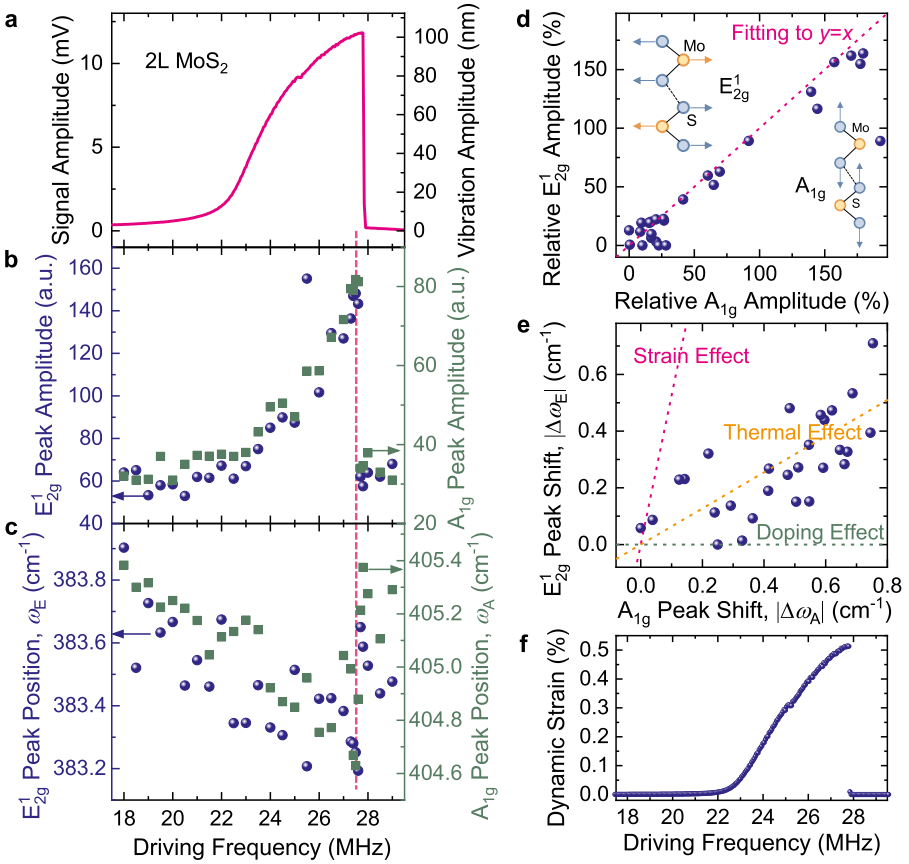

Figure 3. Resonance and Raman mode characteristics measured from the same 2L MoS_2 resonator as shown in Figure 1. (a) Measured nonlinear resonance spectrum of the 2L MoS_2 resonator with d = 4 μm. (b) Measured Raman peak amplitudes at different driving frequencies for $E_{2g}{}^1$ mode (blue symbols, left axis), and A_{1g} mode (green symbols, right axis) with the dashed magenta line showing the transition point of the Duffing nonlinear resonance. (c) Measured Raman peak positions at different driving frequencies for $E_{2g}{}^1$ mode ω_E (blue symbols, left axis), and A_{1g} mode ω_A (green symbols, right axis). (d) The extracted relationship between the relative change of $E_{2g}{}^1$ peak and A_{1g} peak amplitude with the insets showing the illustrations of the atomic displacements for the phonon modes. (e) The extracted relationship between $E_{2g}{}^1$ peak shift ($\Delta\omega_E$) and A_{1g} peak shift ($\Delta\omega_A$) with the effect from different mechanisms shown by the dashed lines. (f) Extracted RF dynamic strain at the largest vibration amplitude of different driving frequencies.

the resonators starts from lithographic patterning and etching of the circular microtrenches on the SiO_2-on-Si wafer. 2D MoS_2 flakes are mechanically exfoliated onto polydimethylsiloxane (PDMS), and then the MoS_2 thickness is identified using an optical microscope and confirmed by peak separation in Raman spectra. 2D MoS_2 layers are then transferred onto selected microtrenches with precise alignment using all-dry transfer techniques that we have developed and optimized,[33] forming circular drumhead 2D MoS_2 NEMS resonators. Finally, by directly evaporating metal through a stencil mask

https://doi.org/10.1021/acs.nanolett.2c01250
Nano Lett. 2022, 22, 5780−5787

with high-precision alignment, metal contact electrodes to the already suspended MoS_2 membranes are made. As such, the process is completely dry without any wet chemical processes that could lead to failure of fabricating suspended membranes. Vibrations of the MoS_2 resonators are excited capacitively by using a DC gate voltage V_{GS} from a power supply and a radio frequency (RF) driving voltage v_{RF} provided by a network analyzer, which are connected to the gate (G) of the device through a bias-tee, with the metal contact (S) to MoS_2 grounded (see Figure 1a). In this measurement system, as we drive the device into motion, not only the mechanical resonance, but also the Raman signal, can be measured, allowing us to probe the dynamical phonon modes. Beside facilitating the driving of device vibrations (linearizing the driving force), the DC gate voltage can also induce strain and control the deflection of MoS_2, as well as change the electron concentration in the suspended MoS_2 through gating and electric field effect.

For a bilayer (2L) MoS_2 NEMS resonator (Figure 1a), we measure linear to nonlinear resonances when gradually increasing v_{RF} from the network analyzer (Figure 1b). We also measure the gate tuning of resonance frequency (Figure 1c), from which the initial strain and gate-induced strain are extracted (see Supporting Information Sections 1−2 for details). With the resonators in Duffing nonlinear resonance regime, the vibration amplitude is much larger than that in the linear regime, as shown by the measured signal amplitude from the photodetector (PD) connected to the network analyzer. As we drive the device into resonance, the Raman spectra are recorded simultaneously with the light first passing through the bandpass filter (BPF) to filter out the resonance signal from the 633 nm laser, and then through the long-pass filter (LPF) to filter out the main 532 nm laser signal. The Raman signal is then collected with the spectrometer (HORIBA Scientific, iHR550), and a liquid-nitrogen-cooled charge-coupled device (CCD). When recording the Raman spectra, we fix the DC and RF driving voltages to ensure enough integration time.

We characterize the dependence of Raman characteristics on varying V_{GS} for the same 2L MoS_2 resonator. With an increasing V_{GS}, we observe decreasing Raman signal amplitudes, and hardening of both E_{2g}^1 and A_{1g} phonon modes (Figure 1d,e). This is in contrast to the effect of gate-induced strain, where a larger gate voltage will lead to softening of phonon modes due to a larger tensile strain. Instead, such decreasing Raman signal amplitude and hardening of the phonon modes can be related to the optical interference effect. V_{GS}-induced deflection changes the interferometry conditions and the optical absorption, leading to a temperature change and thus a Raman peak shift (see Figure S3 for details).

For the same 2L MoS_2 NEMS resonator, we observe Raman amplitude increase and Raman mode softening when driving the device on resonance (Figure 2). The driving force is proportional to $V_{GS}\cdot v_{RF}$, and we observe that when we increase $V_{GS}\cdot v_{RF}$, although the resonance signal amplitude does not increase linearly due to the nonlinear resonance, the resonance signal amplitude for nonlinear resonance at V_{GS} = 10 V, v_{RF} = 1.2 V is still much larger than that for the linear resonance at V_{GS} = 0.1 V, v_{RF} = 1 V (Figure 2a). This results in a shift of the Raman peak position to a smaller wavenumber and an increase of the Raman peak intensity when driving on the nonlinear resonance, compared with those when driving on the linear resonance (Figure 2c). Further, when driving at large amplitude but off resonance, the Raman peak position remains similar to those with a small driving voltage or with no driving, which shows that when the vibration amplitude is not large enough, there will be no measurable Raman shift. When driving the device on resonance, the Raman mode also softens compared with that when driving off resonance (Figure 2b).

By sweeping the frequency around the device resonance frequency while recording the Raman spectra at different driving frequencies, we find that the Raman peak characteristics very well follow the nonlinear resonance amplitude (Figure 3). The nonlinear resonance response can be described using the Duffing equation (by including a cubic term αz^3 in the nonlinear restoring force term):[10,34]

$$\ddot{z} + \gamma\dot{z} + \omega_0^2 z + \alpha z^3 = F(t)/m \tag{1}$$

where z is the displacement in the out-of-plane direction, ω_0 is the angular resonance frequency, $F(t)$ is the external RF driving force, m is the effective modal mass, $\gamma = \omega_0/Q$ is the energy dissipation rate with Q being the quality factor, α is the nonlinear stiffness for the cubic term of displacement. For a resonator with a large vibration amplitude, because the electrostatic force from the gate breaks the symmetry of potential due to deflection, the equilibrium position is dependent on the vibration amplitude.[35] Such change in equilibrium position will change the average vacuum gap, thus changing the optical interferometry condition between the 2D membrane and the substrate, and leading to a change in the Raman signal amplitude. As shown in Figure 3a,b,d, the Raman peak amplitude increases with a larger resonance signal amplitude. During the upward frequency sweep, Duffing nonlinearity with hardening is observed, and the Raman peaks' amplitudes for both E_{2g}^1 mode and A_{1g} mode increase with larger resonance signal amplitude, which indicates an increase in the transduction responsivity of interferometry. When the resonance amplitude drops at the transition point, the Raman peak amplitudes drop as well, showing a strong correlation. The relationship between the relative intensity increase of E_{2g}^1 mode and A_{1g} mode at different driving frequencies in Figure 3d shows that the relative amounts of increase in peak amplitudes are similar as shown by the $y = x$ fitting, which indicates that the change of interferometry condition has similar effects upon these two Raman modes.

In addition, the vibration induces dynamic tensile strain in 2D MoS_2. The tensile strain will result in softening of the phonon mode, and thus a Raman peak position shift to smaller wavenumbers, as shown in previous quasi-static tensile strain measurements.[24,26] This provides us a powerful method for probing the vibration-induced dynamic strain in 2D NEMS resonators. For the 2L MoS_2 NEMS resonator shown in Figure 1, when the frequency approaches the resonance frequency, the vibration amplitude increases, and the Raman modes shift to smaller wavenumbers (Figure 3c). After the transition point for the Duffing nonlinear resonance, the Raman mode shifts to larger wavenumbers, and the largest Raman peak softening is about 0.7 cm^{-1} for E_{2g}^1 mode, and about 0.8 cm^{-1} for A_{1g} mode. Compared with graphene whose Raman peak position has a strain responsivity of −21 cm^{-1}/% strain to −61 cm^{-1}/% strain,[36,37] MoS_2 has a smaller responsivity to strain, making the detection of MoS_2 Raman shift under strain more challenging. Nevertheless, by driving the MoS_2 resonators into strongly nonlinear regime, and detecting the Raman peaks using the 2400 gr/mm blazed holographic grating, we increase the dynamic strain as well as the detection resolution, which

https://doi.org/10.1021/acs.nanolett.2c01250
Nano Lett. 2022, 22, 5780−5787

allows the detection of the Raman peak shift during nanomechanical resonance.

We estimate the dynamic strain induced at different driving frequencies (Figure 3f). We first estimate the critical amplitude using the extracted DC tensile strain from the frequency tuning characteristics. The critical amplitude corresponds to the largest amplitude in the measured resonance spectrum (as shown in Figure 1b) when the nonlinearity just occurs. We then determine the conversion factor or the transduction responsivity of the measured resonance signal amplitude (in millivolts) to the device vibration amplitude (in nanometers) (see Supporting Information Section 3 for details). With the vibration amplitudes at different driving frequencies, we then estimate the corresponding dynamic strain and obtain the largest dynamic strain of 0.51% (Figure 3f), which is detailed in Supporting Information Section 5.

For E_{2g}^1 Raman mode which has been reported to be sensitive to tensile strain, the average dynamic strain can lead to phonon softening, with a strain responsivity of −2.1 cm^{-1}/% strain for 1L MoS_2, and −1.7 cm^{-1}/% strain for few-layer MoS_2.[38] However, A_{1g} mode has been previously reported to be much less sensitive to DC tensile strain with a strain responsivity of only −0.4 cm^{-1}/% strain. Because the measured softening for A_{1g} mode is quite similar to E_{2g}^1 mode (Figure 3c−f), the softening may not be explained by the strain effect alone. Indeed, when the mechanical vibration of such resonant 2D NEMS is coupled with the phonon modes, multiple physical effects are occurring, and we can model the total Raman shift on resonance based on three effects: dynamic strain effect, thermal effect, and doping effect. We can describe this relationship using

$$\Delta\omega = \mathfrak{R}_{\text{Strain}}\cdot\varepsilon_{\text{dynamic}} + \mathfrak{R}_{\text{Thermal}}\cdot\Delta T + \mathfrak{R}_{\text{Doping}}\cdot\Delta n \quad (2)$$

where $\Delta\omega$ is the total Raman peak position shift for certain mode during vibration, $\mathfrak{R}_{\text{Strain}}$ is the responsivity of Raman shift under dynamic strain, $\varepsilon_{\text{dynamic}}$ is the dynamic strain, $\mathfrak{R}_{\text{Thermal}}$ is the responsivity of Raman shift under temperature change, ΔT is the temperature change, $\mathfrak{R}_{\text{Doping}}$ is the responsivity of Raman shift under change in carrier concentration, and Δn is the change in electron concentration.

When the vibration amplitude is large, there will be shift in equilibrium position, which will not only lead to change in interferometry condition and Raman signal intensity, but also result in change in optical absorption and thus the temperature of the membrane. Because of thermal expansion, when the temperature increases, the phonon modes show softening. Because thermal expansion affects both in-plane and out-of-plane modes, $\mathfrak{R}_{\text{Thermal}}$ values for E_{2g}^1 and A_{1g} phonon modes are similar, with 2L MoS_2 showing $\mathfrak{R}_{\text{Thermal}}$ of −0.7 cm^{-1}/100 °C for E_{2g}^1 mode, and −1.1 cm^{-1}/100 °C for A_{1g} mode.[39] Further, during vibration, the vacuum gap periodically changes, leading to change in electron concentration. The charge concentration changes due to the capacitance change, which is a nonlinear function of the vacuum gap change, leading to an averaged doping effect when the MoS_2 periodically vibrates up and down. An increase in n doping will result in softening of A_{1g} phonon mode.[28,29] For the Raman modes E_{2g}^1 and A_{1g} in MoS_2, while they both show softening during resonant motion, the dominant mechanisms for these two modes are different. For E_{2g}^1 mode, the dynamic strain effect and thermal effect are dominant, whereas for A_{1g} mode, the doping effect and thermal effect are dominant, as shown in Figure S5 in the Supporting Information.

For a 3L MoS_2 resonator, the correlation between the Raman characteristics and the resonance signal is also observed (Figure 4). With a larger resonance signal amplitude, the

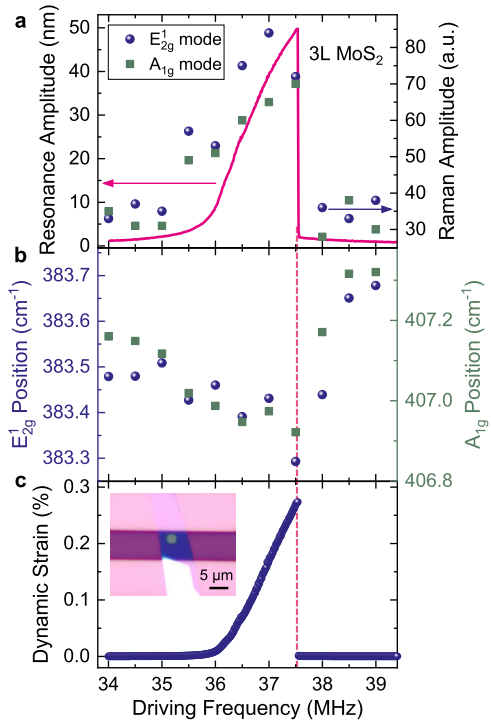

Figure 4. Resonance and Raman peak characteristics measured from the 3L MoS_2 resonator with d = 3 μm, using V_{GS} = 40 V, and v_{RF} = 0.2 V. (a) Measured nonlinear resonance spectrum (magenta line, left axis), and Raman peak amplitudes at different driving frequencies for E_{2g}^1 and A_{1g} modes (blue and green symbols, right axis). (b) Measured Raman peak positions at different driving frequencies for E_{2g}^1 mode (blue symbols, left axis) and A_{1g} mode (green symbols, right axis) with the dashed magenta line showing the transition point of the Duffing nonlinear resonance. (c) Extracted RF dynamic strain at different driving frequencies.

Raman peak intensity increases (Figure 4a), and the peak position shows a consistent shift toward smaller wavenumbers with the largest peak shift of −0.39 cm^{-1} (Figure 4b), which is consistent with the 2L device, further confirming the observed correlation between the Raman and resonance signal. We estimate the largest dynamic strain to be 0.25% (see Supporting Information Section 5 for details).

The Raman characteristics on mechanical resonance is further characterized for a single-layer (1L) MoS_2 resonator with a local gate electrode (Figure 5a). Linear to Duffing nonlinear resonances (Figure 5b), frequency tuning characteristics (Figure 5c), as well as thermomechanical motion (Figure 5d), are observed. Then the doping effect on Raman characteristics is measured by focusing the laser on the substrate-supported region of the MoS_2 while varying the local gate DC voltage V_{GS} (Figure 5e−h). The E_{2g}^1 mode is relatively insensitive to doping, while A_{1g} peak shifts toward lower wavenumbers with increasing n doping at larger V_{GS} (Figure 5e,f), which is consistent with previous reports.[28,29] For the suspended region (Figure 5g,h), the Raman peaks show similar trends as in Figure 1d,e, with a larger V_{GS} leading

https://doi.org/10.1021/acs.nanolett.2c01250
Nano Lett. 2022, 22, 5780−5787

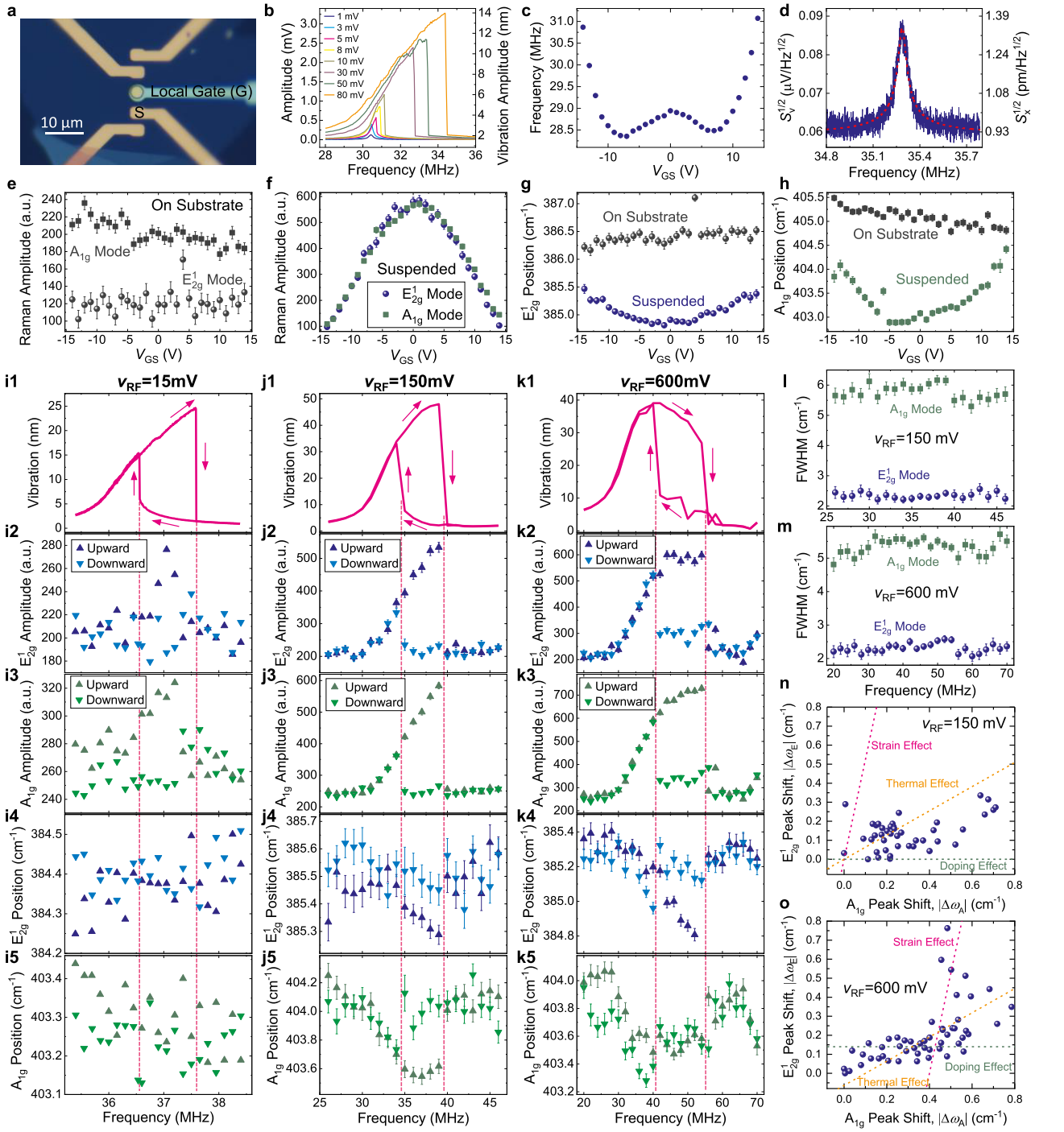

Figure 5. Resonances and Raman spectra measured from a 1L circular drumhead MoS_2 NEMS resonator with d = 3 μm. (a) Optical image of the MoS_2 NEMS resonator with a local gate electrode and contact electrodes. (b) Resonance spectra measured with V_{GS} = 10 V and increasing v_{RF} showing linear to nonlinear resonances, with the corresponding vibration amplitude shown on the right axis. (c) Frequency tuning using V_{GS} with v_{RF} fixed at 2 mV. (d) Undriven thermomechanical noise spectrum with the left axis denoting the measured noise voltage spectral density, and the right axis showing the thermomechanical displacement spectral density. (e–h) Raman characteristics at different V_{GS}, while maintaining v_{RF} = 0 V, showing $E_{2g}{}^1$ and A_{1g} Raman peak amplitudes for (e) the MoS_2 supported on substrate, (f) the suspended MoS_2 membrane, as well as showing (g) $E_{2g}{}^1$ and (h) A_{1g} Raman peak positions for suspended and substrate-supported MoS_2. (i1–i5) Raman responses when measured at V_{GS} = 10 V and v_{RF} = 15 mV showing (i1) the resonance amplitude during upward and downward frequency sweeps, (i2) $E_{2g}{}^1$ Raman peak amplitude, (i3) A_{1g} Raman peak amplitude, (i4) $E_{2g}{}^1$ Raman peak position, and (i5) A_{1g} Raman peak position, at different driving frequencies. (j1–j5) Raman responses shown in the same sequence as in (i1–i5) but with v_{RF} = 150 mV. (k1–k5) Raman responses shown in the same sequence as in (i1–i5) but with v_{RF} = 600 mV. (l–o) FWHM for $E_{2g}{}^1$ and A_{1g} Raman peaks when v_{RF} is (l) 150 mV, and (m) 600 mV. (n–o) Summary of $E_{2g}{}^1$ and A_{1g} peak shifts when v_{RF} is (n) 150 mV, and (o) 600 mV.

to a lower Raman signal amplitude and a shift of Raman modes toward larger wavenumbers. When driven into vibration, we measure the Raman signal during both upward and downward frequency sweeps, for v_{RF} = 15 mV (Figure 5i1–i5), v_{RF} = 150

https://doi.org/10.1021/acs.nanolett.2c01250
Nano Lett. 2022, 22, 5780–5787

mV (Figure 5j1−j5), and ν_{RF} = 600 mV (Figure 5k1−k5). We demonstrate that for small driving at ν_{RF} = 15 mV, only the Raman amplitude shows increase at resonance (Figure 5i1−i3), while the Raman peak positions do not show observable changes (Figure 5i4−i5). At increasing driving of ν_{RF} = 150 mV, phonon mode softening for upward sweep is clearly observed due to larger vibration amplitude (Figure 5j1−j5). When the driving reaches ν_{RF} = 600 mV, both upward and downward frequency sweeps show phonon softening effects, with a maximum peak shift of about −0.8 cm^{-1} (Figure 5k1−k5). The full width at half maximum (FWHM) of Raman peaks during vibration are also characterized, showing widening of the FWHM during resonance for both $E_{2g}{}^1$ and A_{1g} modes due to the averaging of high-frequency mechanical vibrations (Figure 5l,m). We also summarize the relationship between $E_{2g}{}^1$ and A_{1g} mode shift (Figure 5n,o) and show that when ν_{RF} = 600 mV with relatively large vibration amplitude, the dynamic strain effect on Raman peak shift is the dominant effect (Figure 5o). This is intriguing because it indicates different physical mechanisms for Raman peak shift could be dominant at different vibration amplitude.

In summary, we have demonstrated coupled measurements of nanomechanical resonances and Raman modes for 1L, 2L, and 3L MoS_2 NEMS resonators. The devices are driven into strongly nonlinear resonance regime so that large enough vibration amplitude can be achieved for reliable measurements of changes in Raman characteristics. We show Raman peak intensity increase and Raman peak softening with larger vibration amplitude. Such a platform with coupled radio frequency collective nanomechanical vibrational modes and terahertz phonon modes provides new possibilities for studying tunable spin qubits, strain rate, electromechanical coupling, lattice temperature, and energy dissipation.

■ ASSOCIATED CONTENT

Supporting Information

The Supporting Information is available free of charge at https://pubs.acs.org/doi/10.1021/acs.nanolett.2c01250.

Gate-induced static deflection and strain in fully clamped 2D resonators, gate tuning of resonance frequency in fully clamped 2D resonators, estimating amplitude and backbone fitting in nonlinear 2D resonators, DC gate dependence of Raman spectra, vibration-induced strain in nonlinear 2D resonators, multiphysics effects when coupling motion with phonon modes, additional devices and measurements (PDF)

■ AUTHOR INFORMATION

Corresponding Authors

Rui Yang − *Department of Electrical Engineering and Computer Science, Case School of Engineering, Case Western Reserve University, Cleveland, Ohio 44106, United States; University of Michigan − Shanghai Jiao Tong University Joint Institute, Shanghai Jiao Tong University, Shanghai 200240, China; School of Electronic Information and Electrical Engineering, Shanghai Jiao Tong University, Shanghai 200240, China;* orcid.org/0000-0002-6163-2904; Email: rui.yang@sjtu.edu.cn

Philip X.-L. Feng − *Department of Electrical Engineering and Computer Science, Case School of Engineering, Case Western Reserve University, Cleveland, Ohio 44106, United States; Department of Electrical and Computer Engineering, Herbert Wertheim College of Engineering, University of Florida, Gainesville, Florida 32611, United States;* orcid.org/0000-0002-1083-2391; Email: philip.feng@ufl.edu

Authors

S M Enamul Hoque Yousuf − *Department of Electrical and Computer Engineering, Herbert Wertheim College of Engineering, University of Florida, Gainesville, Florida 32611, United States*

Jaesung Lee − *Department of Electrical Engineering and Computer Science, Case School of Engineering, Case Western Reserve University, Cleveland, Ohio 44106, United States; Department of Electrical and Computer Engineering, Herbert Wertheim College of Engineering, University of Florida, Gainesville, Florida 32611, United States*

Pengcheng Zhang − *University of Michigan − Shanghai Jiao Tong University Joint Institute, Shanghai Jiao Tong University, Shanghai 200240, China*

Zuheng Liu − *University of Michigan − Shanghai Jiao Tong University Joint Institute, Shanghai Jiao Tong University, Shanghai 200240, China*

Complete contact information is available at: https://pubs.acs.org/10.1021/acs.nanolett.2c01250

Notes

The authors declare no competing financial interest.

■ ACKNOWLEDGMENTS

We thank the financial support from National Science Foundation (NSF) CAREER Award (Grants ECCS-1454570, ECCS-2015708) and EPMD Program (Grant ECCS-2015670). R.Y., P. Z., and Z.L. are grateful to the financial support from National Natural Science Foundation of China (NSFC) (Grants 62104140, U21A20505), Science and Technology Commission of Shanghai Municipality (STCSM) Natural Science Project General Program (Grant 21ZR1433800), and Shanghai Sailing Program (Grant 19YF1424900).

■ REFERENCES

(1) Lee, C.; Wei, X.; Kysar, J. W.; Hone, J. Measurement of the elastic properties and intrinsic strength of monolayer graphene. *Science* **2008**, *321*, 385−388.

(2) Bertolazzi, S.; Brivio, J.; Kis, A. Stretching and breaking of ultrathin MoS_2. *ACS Nano* **2011**, *5*, 9703−9709.

(3) Bunch, J. S.; van der Zande, A. M.; Verbridge, S. S.; Frank, I. W.; Tanenbaum, D. M.; Parpia, J. M.; Craighead, H. G.; McEuen, P. L. Electromechanical resonators from graphene sheets. *Science* **2007**, *315*, 490−493.

(4) De Alba, R.; Massel, F.; Storch, I. R.; Abhilash, T. S.; Hui, A.; McEuen, P. L.; Craighead, H. G.; Parpia, J. M. Tunable phonon-cavity coupling in graphene membranes. *Nat. Nanotechnol.* **2016**, *11*, 741−746.

(5) Chen, C.; Rosenblatt, S.; Bolotin, K. I.; Kalb, W.; Kim, P.; Kymissis, I.; Stormer, H. L.; Heinz, T. F.; Hone, J. Performance of monolayer graphene nanomechanical resonators with electrical readout. *Nat. Nanotechnol.* **2009**, *4*, 861−867.

(6) Mathew, J. P.; Patel, R. N.; Borah, A.; Vijay, R.; Deshmukh, M. M. Dynamical Strong coupling and parametric amplification of mechanical modes of graphene drums. *Nat. Nanotechnol.* **2016**, *11*, 747−751.

(7) Xu, Y.; Chen, C.; Deshpande, V. V.; DiRenno, F. A.; Gondarenko, A.; Heinz, D. B.; Liu, S.; Kim, P.; Hone, J. Radio frequency electrical transduction of graphene mechanical resonators. *Appl. Phys. Lett.* **2010**, *97*, 243111.

(8) Chen, C.; Lee, S.; Deshpande, V. V.; Lee, G.-H.; Lekas, M.; Shepard, K.; Hone, J. Graphene mechanical oscillators with tunable frequency. *Nat. Nanotechnol.* **2013**, *8*, 923−927.
(9) Lee, J.; Wang, Z.; He, K.; Shan, J.; Feng, P. X.-L. High frequency MoS_2 nanomechanical resonators. *ACS Nano* **2013**, *7*, 6086−6091.
(10) Lee, J.; Wang, Z.; He, K.; Yang, R.; Shan, J.; Feng, P. X.-L. Electrically tunable single- and few-layer MoS_2 nanoelectromechanical systems with broad dynamic range. *Sci. Adv.* **2018**, *4*, No. eaao6653.
(11) Morell, N.; Reserbat-Plantey, A.; Tsioutsios, I.; Schädler, K. G.; Dubin, F.; Koppens, F. H. L.; Bachtold, A. High quality factor mechanical resonators based on WSe_2 monolayers. *Nano Lett.* **2016**, *16*, 5102−5108.
(12) Zhang, P.; Jia, Y.; Shen, S.; Yang, R. Strain-modulated equivalent circuit model and dissipation model for 2D MoS_2 NEMS resonators. 2021 IEEE 34th International Conference on Micro Electro Mechanical Systems (MEMS), Gainesville, FL, USA. January 25−29, 2021; pp 658−661.
(13) Zhang, P.; Jia, Y.; Xie, M.; Liu, Z.; Shen, S.; Wei, J.; Yang, R. Strain-modulated dissipation in two-dimensional molybdenum disulfide nanoelectromechanical resonators. *ACS Nano* **2022**, *16*, 2261−2270.
(14) Manzeli, S.; Allain, A.; Ghadimi, A.; Kis, A. Piezoresistivity and strain-induced band gap tuning in atomically thin MoS_2. *Nano Lett.* **2015**, *15*, 5330−5335.
(15) Yang, R.; Islam, A.; Feng, P. X.-L. Electromechanical coupling and design considerations in single-layer MoS_2 suspended-channel transistors and resonators. *Nanoscale* **2015**, *7*, 19921−19929.
(16) Samanta, C.; Yasasvi Gangavarapu, P. R.; Naik, A. K. Nonlinear mode coupling and internal resonances in MoS_2 nanoelectromechanical system. *Appl. Phys. Lett.* **2015**, *107*, 173110.
(17) Yang, R.; Wang, Z.; Feng, P. X.-L. All-electrical readout of atomically-thin MoS_2 nanoelectromechanical resonators in the VHF band. 2016 IEEE 29th International Conference on Micro Electro Mechanical Systems (MEMS), Shanghai, China. January 24−28, 2016; pp 59−62.
(18) Manzeli, S.; Dumcenco, D.; Migliato Marega, G.; Kis, A. Self-sensing, tunable monolayer MoS_2 nanoelectromechanical resonators. *Nat. Commun.* **2019**, *10*, 4831.
(19) Zhu, J.; Zhang, P.; Yang, R.; Wang, Z. Analyzing electrostatic modulation of signal transduction efficiency in MoS_2 nanoelectromechanical resonators with interferometric readout. *Sci. China Inf. Sci.* **2022**, *65*, 122409.
(20) Ovartchaiyapong, P.; Lee, K. W.; Myers, B. A.; Jayich, A. C. B. Dynamic strain-mediated coupling of a single diamond spin to a mechanical resonator. *Nat. Commun.* **2014**, *5*, 4429.
(21) Yeo, I.; de Assis, P-L.; Gloppe, A.; Dupont-Ferrier, E.; Verlot, P.; Malik, N. S.; Dupuy, E.; Claudon, J.; Gerard, J-M.; Auffeves, A.; Nogues, G.; Seidelin, S.; Poizat, J-P.; Arcizet, O.; Richard, M. Strain-mediated coupling in a quantum dot−mechanical oscillator hybrid system. *Nat. Nanotechnol.* **2014**, *9*, 106−110.
(22) Maity, S.; Shao, L.; Bogdanović, S.; Meesala, S.; Sohn, Y.-I.; Sinclair, N.; Pingault, B.; Chalupnik, M.; Chia, C.; Zheng, L.; Lai, K.; Lončar, M. Coherent acoustic control of a single silicon vacancy spin in diamond. *Nature Commun.* **2020**, *11*, 193.
(23) He, K.; Poole, C.; Mak, K. F.; Shan, J. Experimental demonstration of continuous electronic structure tuning via strain in atomically thin MoS_2. *Nano Lett.* **2013**, *13*, 2931−2936.
(24) Conley, H. J.; Wang, B.; Ziegler, J. I.; Haglund, R. F., Jr; Pantelides, S. T.; Bolotin, K. I. Bandgap engineering of strained monolayer and bilayer MoS_2. *Nano Lett.* **2013**, *13*, 3626−3630.
(25) Zhu, C. R.; Wang, G.; Liu, B. L.; Marie, X.; Qiao, X. F.; Zhang, X.; Wu, X. X.; Fan, H.; Tan, P. H.; Amand, T.; Urbaszek, B. Strain tuning of optical emission energy and polarization in monolayer and bilayer MoS_2. *Phys. Rev. B: Condens. Matter Mater. Phys.* **2013**, *88*, 121301.
(26) Yang, R.; Lee, J.; Ghosh, S.; Tang, H.; Sankaran, R. M.; Zorman, C. A.; Feng, P. X.-L. Tuning optical signatures of single-and few-layer MoS_2 by blown-bubble bulge straining up to fracture. *Nano Lett.* **2017**, *17*, 4568−4575.
(27) Blundo, E.; Cappelluti, E.; Felici, M.; Pettinari, G.; Polimeni, A. Strain-tuning of the electronic, optical, and vibrational properties of two-dimensional crystals. *Appl. Phys. Rev.* **2021**, *8*, 021318.
(28) Lu, X.; Utama, M. I. B.; Wang, X.; Xu, W.; Zhao, W.; Owen, M. H. S.; Xiong, Q. Gate-tunable resonant Raman spectroscopy of bilayer MoS_2. *Small* **2017**, *13*, 1701039.
(29) Chakraborty, B.; Bera, A.; Muthu, D. V. S.; Bhowmick, S.; Waghmare, U. V.; Sood, A. K. Symmetry-dependent phonon renormalization in monolayer MoS_2 transistor. *Phys. Rev. B* **2012**, *85*, 161403.
(30) Reserbat-Plantey, A.; Marty, L.; Arcizet, O.; Bendiab, N.; Bouchiat, V. A local optical probe for measuring motion and stress in a nanoelectromechanical system. *Nat. Nanotechnol.* **2012**, *7*, 151−155.
(31) Zhang, X.; Makles, K.; Colombier, L.; Metten, D.; Majjad, H.; Verlot, P.; Berciaud, S. Dynamically-enhanced strain in atomically thin resonators. *Nat. Commun.* **2020**, *11*, 5526.
(32) Xie, H.; Jiang, S.; Rhodes, D. A.; Hone, J. C.; Shan, J.; Mak, K. F. Tunable exciton-optomechanical coupling in suspended monolayer $MoSe_2$. *Nano Lett.* **2021**, *21*, 2538−2543.
(33) Yang, R.; Zheng, X.; Wang, Z.; Miller, C. J.; Feng, P. X.-L. Multilayer MoS_2 transistors enabled by a facile dry-transfer technique and thermal annealing. *J. Vac. Sci. Technol. B* **2014**, *32*, 061203.
(34) Czaplewski, D. A.; Strachan, S.; Shoshani, O.; Shaw, S. W.; López, D. Bifurcation diagram and dynamic response of a MEMS resonator with a 1:3 internal resonance. *Appl. Phys. Lett.* **2019**, *114*, 254104.
(35) Eichler, A.; Moser, J.; Dykman, M. I.; Bachtold, A. Symmetry breaking in a mechanical resonator made from a carbon nanotube. *Nat. Commun.* **2013**, *4*, 2843.
(36) Huang, M.; Yan, H.; Heinz, T. F.; Hone, J. Probing strain-induced electronic structure change in graphene by Raman spectroscopy. *Nano Lett.* **2010**, *10*, 4074−4079.
(37) Young, R. J.; Gong, L.; Kinloch, I. A.; Riaz, I.; Jalil, R.; Novoselov, K. S. Strain mapping in a graphene monolayer nanocomposite. *ACS Nano* **2011**, *5*, 3079−3084.
(38) Rice, C.; Young, R. J.; Zan, R.; Bangert, U.; Wolverson, D.; Georgiou, T.; Jalil, R.; Novoselov, K. S. Raman-scattering measurements and first-principles calculations of strain-induced phonon shifts in monolayer MoS_2. *Phys. Rev. B* **2013**, *87*, 081307.
(39) Lin, Z.; Liu, W.; Tian, S.; Zhu, K.; Huang, Y.; Yang, Y. Thermal expansion coefficient of few-layer MoS_2 studied by temperature-dependent Raman spectroscopy. *Sci. Rep.* **2021**, *11*, 7037.

NOTE ADDED AFTER ASAP PUBLICATION

This paper published ASAP on July 6, 2022 with errors in the Supporting Information. The errors were corrected and the updated files published on July 7, 2022.

https://doi.org/10.1021/acs.nanolett.2c01250
Nano Lett. 2022, 22, 5780−5787